A Local Level Set Method for Paraxial Geometrical Optics

Jianliang Qian* Shingyu Leung†

November 4, 2003

Abstract

We propose a local level set method for constructing the geometrical optics term in the paraxial formulation for the high frequency asymptotics of 2-D acoustic wave equations. The geometrical optics term consists of two multivalued functions: a traveltime function satisfying the eikonal equation locally and an amplitude function solving a transport equation locally. The multivalued traveltimes are obtained by solving a level set equation and a traveltime equation with a forcing term. The multivalued amplitudes are computed by a new Eulerian formula based on the gradients of traveltimes and takeoff angles. As a byproduct the method is also able to capture the caustic locations. The proposed Eulerian method has complexity of $O(N^2 LogN)$, rather than $O(N^4)$ as typically seen in the Lagrangian ray tracing method. Several examples including the well known Marmousi synthetic model illustrate the accuracy and efficiency of the Eulerian method.

1 Introduction

Geometrical optics is the branch of optics which is characterized by the neglect of the wavelength, i.e. that corresponding to the limiting case (wavelength) going to zero ("short wavelength"), or equivalently for the wave number near infinity ("high frequency"), since in this approximation the optical laws may be formulated in the language of geometry [5]. This definition is based on short wavelength assumption of light and can be generalized to deal with other wave phenomena as well. The linear or nonlinear partial differential equations describing these wave propagations involve a parameter, such as the wavelength λ, which is small compared to all other lengths in the problem [43]. The asymptotic method is for the asymptotic solution of PDEs governing these wave propagations.

Consider the linear acoustic wave equation. According to the Debye procedure, inserting the high frequency asymptotic ansatz into the wave equation reduces the resolution of the

*Department of Mathematics, UCLA, Los Angeles, CA 90095-1555. Email: **qian@math.ucla.edu**

†Department of Mathematics, UCLA, Los Angeles, CA 90095-1555. Email: **syleung@math.ucla.edu**

PDE into the resolution for a sequence of ODEs. Among all the terms in the asymptotic ansatz, the most important term is the zeroth order term, the so-called geometrical optics term [21]. The geometrical optics term consists of two functions, a phase function satisfying the eikonal equation, a first-order nonlinear PDE, and an amplitude function solving a linear transport equation with the phase gradient as coefficients. Thus to construct the geometrical optics term the eikonal equation has to be solved first for the phase function; then the transport equation for amplitude might be integrated afterwards.

Conventionally, the eikonal equation was solved by the method of characteristics, a.k.a. the ray tracing method in the seismology and optics; thus the method inherits the intrinsic shortcoming of the Lagrangian method, i.e. the non-uniform resolution in the desired computational domain. In this setup, the amplitude function could be obtained by solving an ODE system as well, and it has the similar shortcoming. Certainly it is possible to overcome this drawback by introducing complicated interpolation and bookkeeping data structures [41]. However, in the late 80's Vidale [40], and van Trier and Symes [39] introduced direct discretizations of the eikonal equation based on finite difference schemes, which are Eulerian approaches and yield uniform resolutions of the solution in the computational domain. As pointed out in [39], the obtained solution should be understood as the minimum phase or the first-arrival traveltime in the viscosity solution sense for Hamilton-Jacobi equations [22]. Once the traveltime is obtained, the transport equation for amplitude might be integrated [44, 37, 31]. Since a viscosity solution usually develops kinks, the gradient of the phase function is discontinuous. Therefore, the resulting solution for the transport equation has to be understood in the measure sense [12]. The difference between the ray tracing solution and the finite difference solution of the eikonal equation is that one is multiple-valued and the other single-valued [3, 10]. Although the viscosity concept and related numerical methods provide a natural Eulerian framework for geometrical optics, the drawback is that it provides only first arrivals while some applications may require all arrival times. Moreover, White [42] proved that there is a high probability for so-called transmission caustics to occur in an inhomogeneous medium. Beyond transmission caustics, more than one ray pass over each point in space so that the phase is multivalued. Therefore, it is important to design Eulerian methods for multivalued solutions of the eikonal equation, in general, the Hamilton-Jacobi equation.

In the last decade or so, there are a lot of efforts in this direction: geometrical domain decomposition type methods [2], slowness matching method [35, 36], dynamic surface extension method [33, 32], segment projection method [11], level set method [25, 29, 9, 19, 8, 30], phase space method [13]. See [3, 10] for up-to-date reviews of the above methods and moment-based methods [15, 18].

In this work we present a local level set method for paraxial geometrical optics. By paraxial we mean that the wave propagation has a spatial orientation so that one of the spatial directions may be viewed as an evolution direction. This criterion may be quantified by assuming a sub-horizontal condition for the eikonal equation [36]. In [30], we presented a global level set method for the paraxial eikonal equation in the 2-dimensional case, and the computed multivalued traveltime matched the ray tracing solution very well even in the difficult synthetic Marmousi model. Therefore we proceed along the same line and

design a fast local level set method for both multivalued traveltimes and amplitudes, thus constructing the geometrical optics term. This construction will be useful for modern high resolution seismic imaging [14, 16, 34, 7, 24]. Our formulation for computing the multivalued amplitude is based upon a level set formulation and an extension of the Eulerian amplitude formulation used in [31], which is different from the one used in [25]. As a by-product, our formulation also yields the cuspoid caustic curves (A_3 type) [38], which is related to the catastrophe theory; thus it suggests that the level set theory can be used to study the catastrophe development. See [4] for another Eulerian method for capturing caustics. The overall complexity of our level set method is $O(N^2 LogN)$ rather than $O(N^4)$ as typically seen in the ray tracing formulation.

The rest of the paper is organized as follows: Section 2 introduces the paraxial formulation for the high frequency asymptotics of 2-D acoustic wave equations; Section 3 presents the level set formulation for wavefront locations, traveltimes, amplitudes and caustics; Section 4 gives implementation details of the local level set method; Section 5 shows some numerical examples to illustrate the efficiency and accuracy of the Eulerian method and Section 6 indicates some possible future works.

2 Paraxial Formulation for Eikonal Equation

Consider the acoustic wave equation

$$\Delta U - \frac{1}{c^2(\mathbf{x})} U_{tt} = 0 \tag{1}$$

where the velocity $c(\mathbf{x}) > 0$ is given. We are interested in the leading singularity of the wave field which is characterized by the following asymptotic solution:

$$U(\mathbf{x}, t) \approx \Sigma_{j=1}^{j=M} A_j(\mathbf{x}) S(t - \tau_j(\mathbf{x})) \tag{2}$$

where S is a given waveform function, and A_j and τ_j are smooth functions to be determined; the number M of the terms in the sum depends on the velocity $c(\mathbf{x})$ and must be determined in the process of constructing the solution [20]; τ_j and A_j in ansatz (2) should be regarded as different branches of two multivalued functions $\tau(\mathbf{x})$ and $A(\mathbf{x})$; each branch is defined on its own domain D_j.

Inserting one term of ansatz (2) into the wave equation and using the Debye procedure, omitting the subscripts, we have the following two equations from the coefficients of S'' and S' [34]:

$$|\nabla \tau| = \frac{1}{c(\mathbf{x})}, \tag{3}$$

$$\nabla \cdot (A^2 \nabla \tau) = 0. \tag{4}$$

Eq. (3) is the so-called eikonal equation for traveltime, and Eq. (4) is the transport equation which says that A^2 is conserved along the ray.

Under appropriate conditions pairs of branches of the solution τ_j are joined along the caustic curves. Therefore the direct resolution approach proposed in [2] first locates these caustic curves, then solves eikonal equations in the corresponding geometrical domains, and finally glues different branches together to obtain multivalued solutions. To avoid the complicated process for locating the caustic curves, we start from the method of characteristics and derive a level-set based Eulerian approach to constructing the geometrical optics term.

Consider a point source condition for the eikonal equation defined in an open, bounded domain $\Omega \subset \mathbf{R}^2$. To emphasize the point source condition the eikonal equation is rewritten as follows,

$$|\nabla_{\mathbf{x}} \tau(\mathbf{x}, \mathbf{x}_s)| = \frac{1}{c(\mathbf{x})}. \tag{5}$$

$$\lim_{\mathbf{x}\to\mathbf{x}_s} \frac{\tau(\mathbf{x}, \mathbf{x}_s)}{\|\mathbf{x} - \mathbf{x}_s\|} = \frac{1}{c(\mathbf{x}_s)}, \ \tau \geq 0, \tag{6}$$

where $\mathbf{x}_s$ is the given source point.

By the method of characteristics for the eikonal equation (5) with the point source condition (6), we have a ray tracing system,

$$\frac{dx}{dt} = c \sin\theta \tag{7}$$

$$\frac{dz}{dt} = c \cos\theta \tag{8}$$

$$\frac{d\theta}{dt} = \sin\theta \frac{\partial c}{\partial z} - \cos\theta \frac{\partial c}{\partial x} \tag{9}$$

with initial conditions

$$x|_{t=0} = x_s \tag{10}$$

$$z|_{t=0} = z_s \tag{11}$$

$$\theta|_{t=0} = \theta_s \tag{12}$$

where $\mathbf{x} = (x, z)$, $\mathbf{x}_s = (x_s, z_s)$ and θ_s varies from $-\pi$ to π. In this system, t has the dimension of time. This is a multivalued Lagrangian formulation because even though the rays in the phase space (x, z, θ) may never intersect, the projected rays in the physical space (x, z) may intersect.

Next we extend the traveltime function $\tau(x, z)$ to the reduced phase space $\{(x, z, \theta)\}$, denoted as $T(x, z, \theta)$, and consider the t-wavefront expanding from the source point:

$$T(x, z, \theta) = t. \tag{13}$$

Differentiating this identity with respect to t we have

$$c \sin\theta \, T_x + c \cos\theta \, T_z + (\sin\theta \frac{\partial c}{\partial z} - \cos\theta \frac{\partial c}{\partial x}) \, T_\theta = 1. \tag{14}$$

In addition, we have the boundary condition

$$T(x_s, z_s, \theta_s) = 0, \qquad -\pi \le \theta_s \le \pi. \tag{15}$$

Since Eq.(14) is a linear advection equation, one may be tempted to solve it directly with the condition (15). However, for a given $(x, z) \neq (x_s, z_s)$, $T(x, z, \cdot)$ is not necessarily well defined for every θ. In other words, Eqs. (14) and (15) are not well-posed. To obtain an efficient well-posed problem, we will assume the paraxial condition and use the level set formulation.

In some applications, for example, wave propagation in reflection seismics, the traveltimes of interest are carried by the so-called sub-horizontal rays [16, 31], where sub-horizontal means "oriented in the positive z-direction". A convenient characterization for sub-horizontal rays is that

$$\frac{dz}{dt} \ge c \cos\theta_{\max} > 0 \tag{16}$$

for some $\theta_{\max}$ with $0 < \theta_{\max} < \frac{\pi}{2}$. This inequality holds for rays making an angle θ with the vertical satisfying $|\theta| \le \theta_{\max} < \frac{\pi}{2}$.

To be specific, consider

$$\Omega \;=\; \{(x, z) : x_{\min} \le x \le x_{\max}, 0 \le z \le z_{\max}\} \tag{17}$$

and assume that the source is located on the surface: $x_{\min} \le x_s \le x_{\max}$ and $z_s = 0$. By the sub-horizontal condition we can use depth z as the running parameter so that we have a reduced system

$$\frac{dx}{dz} \;=\; \tan\theta \tag{18}$$

$$\frac{d\theta}{dz} \;=\; \frac{1}{c}\left(\frac{\partial c}{\partial z}\tan\theta - \frac{\partial c}{\partial x}\right) \tag{19}$$

with

$$x|_{z=0} \;=\; x_s \tag{20}$$

$$\theta|_{z=0} \;=\; \theta_s \tag{21}$$

where now θ_s varies from $-\theta_{\max} \le \theta \le \theta_{\max} < \frac{\pi}{2}$. In addition, the traveltime is computed by integrating

$$\frac{dt}{dz} \;=\; \frac{1}{c\cos\theta} \tag{22}$$

with

$$t|_{z=0} \;=\; 0. \tag{23}$$

This ray tracing system (18-21) is a multivalued Lagrangian formulation defined in the reduced phase space $(z; x, \theta)$. Actually, the ray tracing system can be obtained by applying the method of characteristics to the paraxial eikonal equation

$$\frac{\partial \tau}{\partial z} = H\left(x, z, \frac{\partial \tau}{\partial x}\right) = \sqrt{\max\left(\frac{1}{c^2} - \left(\frac{\partial \tau}{\partial x}\right)^2, \frac{\cos^2\theta_{\max}}{c^2}\right)}, \tag{24}$$

which in turn comes from enforcing the sub-horizontal condition in the eikonal equation (5); see [36] for a theoretical justification. In this equation, τ has the dimension of time too; therefore it is identical to t.

As we will see, since the ray tracing system (18), (19) is formulated in a reduced phase space, we may use a level set motion equation to move the initial curve deduced from the initial condition and the curves moved will not self-intersect because they are defined in the reduced phase space.

3 Level Set Formulation

3.1 Level set equation for wavefronts

By the paraxial assumption, we treat z as an artificial time variable. Now, if we define $\phi = \phi(z, x, \theta)$ such that the zero level set, $\{(x(z), \theta(z)) : \phi(z, x(z), \theta(z)) = 0\}$, gives the location of the reduced bicharacteristic strip $(x(z), \theta(z))$ at z, then we may differentiate the zero level set equation with respect to z to obtain

$$\phi_z + u\phi_x + v\phi_\theta = 0, \tag{25}$$

with

$$u = \frac{dx}{dz} \text{ and } v = \frac{d\theta}{dz}, \tag{26}$$

which are given by the ray equations (18-19). In essence, we embed the ray tracing equations as the velocity field, $\mathbf{u} = (u, v)$, into the level set equation which governs the motion of the bicharacteristic strips in the phase space.

The initial condition for the level set motion equation (25) is taken to be

$$\phi|_{z=0} = \phi(0, x, \theta) = x - x_s, \tag{27}$$

which is obtained from initial conditions (20) and (21). This is a signed distance function, satisfying $|\nabla_{x,\theta}\phi| = 1$, to the initial phase space curve

$$\{(x, \theta) : x = x_s, -\theta_{\max} \le \theta \le \theta_{\max}\} \tag{28}$$

in the reduced phase space

$$\Omega_p = \{(x, \theta) : x_{\min} \le x \le x_{\max}, -\theta_{\max} \le \theta \le \theta_{\max}\}. \tag{29}$$

The initial curve partitions Ω_p into two sub-domains represented by $\{(x,\theta) : \phi(0,\cdot,\cdot) < 0\}$ and $\{(x,\theta) : \phi(0,\cdot,\cdot) > 0\}$. Afterwards, the level set motion equation takes over and moves this initial curve as z varies, and the zero level set of ϕ at z gives the location of the new curve which still partitions Ω_p into two sub-domains. Since the initial curve defines an implicit function between x and θ, where θ is a (possibly multivalued) function of x, the new curve shares the same property. As the curve moves under the given velocity, it may develop overturning. Therefore, for a fixed z, for some x's we may have more than one θ^* such that $\phi(z,x,\theta^*) = 0$. This essentially tells us where the solutions are multivalued. On the zero level set, when $\phi_\theta \neq 0$, there exists local unique projection on to the x-space; when $\phi_\theta = 0$, the corresponding singularities or catastrophes of the implicit function $\theta = \theta(z,x)$ for fixed z's are identified as caustics [38].

3.2 Traveltime

To determine the traveltime of the ray from the above level set equation, we now derive a corresponding equation governing the evolution of the traveltime. By the sub-horizontal condition in the paraxial formulation and the ray equation (22), let $F_{\mathbf{u}}(x,\theta;z)$ be the flow generated by the velocity field $\mathbf{u}$ in the phase space (x,θ) along the z-direction. Thus we can write

$$\frac{dT}{dz}(z, F_{\mathbf{u}}(x,\theta;z)) \;=\; \frac{1}{c\cos\theta}\,. \tag{30}$$

Therefore, having $t = T(z,x,\theta)$ we get the following advection equation

$$\frac{dt}{dz} \;=\; \frac{dT}{dz} = T_z + uT_x + vT_\theta = \frac{1}{c\cos\theta}\,. \tag{31}$$

This equation can also be derived from Eq. (14) directly.

The initial condition for T is specified according to the initial condition (23):

$$T|_{z=0} \;=\; T(0,x,\theta) = 0\,, \tag{32}$$

which is consistent with the initial condition (27).

3.3 Amplitude

The amplitude of the ray can be computed according to the formula given in [44, 31]:

$$\tilde{A}(x,z;x_s,z_s) = \frac{1}{2\pi}\sqrt{\frac{c}{2}}\sqrt{|\nabla\tilde{T}\times\nabla\tilde{\psi}|}\;, \tag{33}$$

where $\tilde{T}$ and $\tilde{\psi}$ are, respectively, the traveltime and the take-off angle of a ray reaching (x,z) from (x_s,z_s). Traveltimes and takeoff angles are well defined on each solution branch in the physical space (x,z). To compute this quantity in the reduced phase space, we consider T as the extension of $\tilde{T}$ to the phase space; furthermore, we may also extend $\tilde{\psi}$ and $\tilde{A}$ to ψ

and A in the (z, x, θ) space, respectively. Since the takeoff angle is constant along a given ray in the phase space, we have

$$\psi_z + u\psi_x + v\psi_\theta = 0\,. \tag{34}$$

Moreover, we have

$$\begin{aligned}
\frac{\partial \tilde{T}}{\partial x} &= T_x + T_\theta \frac{\partial \theta}{\partial x}\,,\\
\frac{\partial \tilde{T}}{\partial z} &= T_z + T_\theta \frac{\partial \theta}{\partial z}\,,\\
\frac{\partial \tilde{\psi}}{\partial x} &= \psi_x + \psi_\theta \frac{\partial \theta}{\partial x}\,,\\
\frac{\partial \tilde{\psi}}{\partial z} &= \psi_x + \psi_\theta \frac{\partial \theta}{\partial z}\,.
\end{aligned} \tag{35}$$

It follows that

$$\left|\nabla \tilde{T} \times \nabla \tilde{\psi}\right| = \left|(T_x\psi_\theta - T_\theta\psi_x)\left(-v + u\frac{\partial \theta}{dx} + \frac{\partial \theta}{\partial z}\right) - \frac{1}{c\cos\theta}\left(\psi_x + \psi_\theta \frac{\partial \theta}{\partial x}\right)\right|\,. \tag{36}$$

Since $\phi(z, x, \theta(x, z)) = 0$ on the zero level set and eq.(19), we have

$$\frac{\partial \theta}{\partial x} = -\frac{\partial \phi/\partial x}{\partial \phi/\partial \theta} \;\text{ and }\; \frac{\partial \theta}{\partial z} = v - u\frac{\partial \theta}{\partial x}\,. \tag{37}$$

Finally we have

$$A(z; x, \theta) = \frac{1}{2\pi}\sqrt{\frac{c}{2\cos\theta}}\sqrt{\left|\frac{\psi_x\phi_\theta - \psi_\theta\phi_x}{\phi_\theta}\right|}\,. \tag{38}$$

To compute the amplitude, we need the derivatives of the level set function at different z's. However, as illustrated in [30], reinitialization of the level set function is necessary and unfortunately, this process would only keep the location of the zero level set unchanged. This means the derivatives of ϕ cannot be computed directly from the level set function by differentiating the function ϕ itself after the regularization procedure. Therefore, to compute the derivatives of the level set function on the zero level set, we need to advect those derivatives as well. We first let $\xi = \phi_x$ and $\eta = \phi_\theta$. Differentiating the advection equation for ϕ with respect to x and θ respectively, we have

$$\begin{aligned}
\xi_z + u\xi_x + v\xi_\theta + u_x\xi + v_x\eta &= 0\,,\\
\eta_z + u\eta_x + v\eta_\theta + u_\theta\xi + v_\theta\eta &= 0\,.
\end{aligned} \tag{39}$$

We might apply the same idea to the advection equation for takeoff angles as well so that the derivatives of takeoff angles could be determined. Once those ingredients are in place, the amplitude could be obtained. However, we will not use this approach because

computationally this is not efficient and numerically it is difficult to reconcile the accuracies of four different derivatives.

Instead, defining

$$\Delta = \psi_x \phi_\theta - \psi_\theta \phi_x \tag{40}$$

and differentiating it with respect to z, we have the advection equation

$$\Delta_z + \nabla_{x,\theta} \cdot (\mathbf{u}\Delta) = 0\,, \tag{41}$$

and the amplitude can then be computed by

$$A(z; x, \theta) = \frac{1}{2\pi} \sqrt{\left| \frac{c}{2\cos\theta} \frac{\Delta}{\phi_\theta} \right|}\,. \tag{42}$$

Therefore, we can simply solve the advection equations for ϕ_x, ϕ_θ and Δ in order to get the amplitude. We need the advection equation for ϕ_x because it is coupled with the one for ϕ_θ.

In general, Δ is a bounded quantity and ϕ_θ may approach zero. When ϕ_θ goes to zero, A goes to ∞ and we are approaching caustics.

3.4 Caustics

Mathematically, caustic surfaces are envelops of the family of rays. In the geometrical optics, at a caustic the amplitude of the asymptotic expansion becomes infinite, so that the usual asymptotic expansion is no longer valid at caustics, and some special expansions have been introduced to construct wave fields near the caustics [23, 6].

In the current level set formulation, the caustic curves correspond to

$$\{(z, x) : \phi(z, x, \theta(x, z)) = 0 \text{ and } \phi_\theta(z, x, \theta(x, z)) = 0\}.$$

4 Implementation

4.1 Boundary Conditions

When solving the advection equations for ϕ, ϕ_x, ϕ_θ, Δ and T, we have to specify suitable boundary conditions.

Because the level set equation is a homogeneous advection equation, a non-reflective boundary condition is used for the level set equation, meaning $\partial\phi/\partial\mathbf{n} = 0$, where $\mathbf{n}$ is the outward normal along the boundary of Ω_p. This ensures the information outside the domain Ω_p will not interfere with the zero level set inside the computational domain. Similarly, non-reflective boundary conditions are enforced on the advection equations for Δ, ϕ_x and ϕ_θ. These in turn can be easily implemented in the upwind schemes used here.

However, since the traveltime equation is a hyperbolic equation with a forcing term, we need to specify normal derivatives of the traveltime along the boundary according to the

characteristic system. In general, there are two types of characteristics, i.e., outgoing and incoming characteristics. By using upwind numerical schemes, those boundary conditions can be taken care of automatically if some appropriate normal derivatives are imposed on the boundary so that the outside information will not propagate into the computational domain. To obtain such normal derivatives, we use the information from the characteristics system. We first invert equation (7) and (9) locally and get

$$\frac{\partial T}{\partial x} = \frac{1}{c\sin\theta}, \tag{43}$$

which is used for boundaries $x = x_{\min}$ and $x = x_{\max}$, and

$$\frac{\partial T}{\partial \theta} = \left(\sin\theta\frac{\partial c}{\partial z} - \cos\theta\frac{\partial c}{\partial x}\right)^{-1}, \tag{44}$$

which is for boundaries $\theta = -\theta_{\max}$ and $\theta = \theta_{\max}$.

The above conditions essentially specify the normal derivatives of traveltime along the boundaries. Then the values of T on the boundaries will be obtained by applying the Adams' Extrapolation formula to equation (43), where θ is considered as fixed, and to equation (44), where x is considered as fixed.

In equation (43), when $\theta = 0$, it seems that there is a singularity. However, in that case, $u = 0$ as well, the singularity is canceled eventually. The purpose for enforcing boundary conditions on T is to avoid outside information propagating into the domain. In practice, we have found that the above strategy works well.

4.2 Regularizations and a global level set method

Initially at $z = 0$, we have a signed distance function satisfying $|\nabla\phi| = 1$, so that the level sets, i.e., contours, of ϕ are equally spaced. However, as z varies the level set equation is solved and the level set function is updated; in general the level set function is no longer equally spaced because of the underlying inhomogeneous velocity field, even though the zero level set of ϕ at z, the curve that we are interested in, is moving at the correct velocity. This implies that ϕ may develop steep and flat gradients at or near the zero level set, making the computed curve locations and further computations inaccurate, which does happen in practice.

Therefore, the following regularization procedure consisting of reinitialization and orthogonalization was proposed in [30].

To restore the equally spaced property for the level sets, the usual way is to make ϕ a signed distance function without moving the zero level set of ϕ appreciably. This can be achieved through the so-called reinitialization by solving the following equation to steady state $\tilde{\phi}_\infty$ [45, 28, 26]:

$$\frac{\partial\tilde{\phi}}{\partial\xi} + S(\phi)(|\nabla\tilde{\phi}| - 1) = 0 \tag{45}$$

$$\tilde{\phi}|_{\xi=0} = \phi(z,\cdot,\cdot). \tag{46}$$

Here $S(\phi)$ could be the smoothed signum function [26]

$$S(\phi) = \frac{\phi}{\sqrt{\phi^2 + |\nabla\phi|^2 \Delta x \Delta\theta}}. \tag{47}$$

where Δx and $\Delta\theta$ are the mesh sizes along x- and θ-directions, respectively.

The steady state $\tilde{\phi}_\infty$ has the same zero level set as $\phi(z,\cdot,\cdot)$ within a certain accuracy since $\tilde{\phi}$ does not move on the zero level set of ϕ. Moreover, at the steady state $\tilde{\phi}_\infty$ is a signed distance function since $|\nabla\tilde{\phi}_\infty| = 1$. The reinitialization step is to use $\tilde{\phi}_\infty$ instead of $\phi(z,\cdot,\cdot)$ as the initial condition at z for solving the level set motion equation to the next stage. To achieve the steady state we usually need to evolve equation (45) for a few steps only. How often we should invoke the reinitialization step is a subtle issue; see [28, 26] for some discussions.

Because we are only interested in the values of T where $\phi = 0$, we propose the following orthogonalization procedure

$$\frac{\partial\hat{T}}{\partial\xi} + \mathrm{sgn}(\phi)\left(\frac{\nabla\phi}{|\nabla\phi|}\cdot\nabla\hat{T}\right) = 0\,, \tag{48}$$

$$\hat{T}|_{\xi=0} = T(z,\cdot,\cdot) \tag{49}$$

which, theoretically, preserves the values of T where $\phi = 0$ but changes them elsewhere so that the new T will not vary too much near the desired region. At the steady state, $\nabla\phi\cdot\nabla\hat{T} = 0$. Equation (48) may also be viewed as an extension procedure; namely, we extend the values of T on the zero level set of ϕ along the normals of the zero level set of ϕ. This generally makes T discontinuous since lines normal to the zero level set will eventually intersect somewhere away from the zero level set. Even if the location of the zero level set may be shifted, the effect to the interpolation will still be acceptable.

The following algorithm first appeared in [30].

Algorithm 1:

I. Initialization.

1. Given N_x and N_θ, determine

$$\Delta x = \frac{x_{\max} - x_{\min}}{N_z - 1} \text{ and } \Delta\theta = \frac{2\theta_{\max}}{N_\theta - 1}\,.$$

2. Initialize ϕ and T at $z = 0$.

II. March in z until $z = z_{\max}$.

1. Determine Δz from the CFL condition.
2. March one Δz step by solving the level set equation (25).
3. Reinitialize the level set function by solving (45).

4. March one Δz step by solving the traveltime equation (31).
5. Orthogonalize T and ϕ by solving equation (48).

III. Output. For each x_i with $i = 1, \ldots, N_x$,

1. Determine **all** root θ_k such that $\phi(z_{\max}, x_i, \theta_k) = 0$ $(k = 1, \cdots)$.
2. Determine $T(z_{\max}, x_i, \theta_k)$ $(k = 1, \cdots)$ by interpolation.

In Step I, the level set equation and the traveltime equation are decoupled and thus can be solved separately. The spacial derivatives are approximated by a fifth-order WENO-Godunov scheme [17] while a third-order TVD-RK method [27] is used for the time marching. Since both the level set equation (25) and the traveltime equation (31) are linear, the CFL step Δz can be chosen by

$$\Delta z \quad \leq \quad \beta \frac{\min(\Delta x, \Delta\theta)}{\max(\sqrt{u^2 + v^2})}, \tag{50}$$

where Δx and $\Delta\theta$ are mesh sizes along x and θ directions, respectively, and β is the CFL number taken to be 0.6. For the root-finding and the interpolation in Step III, we can simply use any non-oscillatory interpolation scheme, for example, a linear interpolation or an ENO reconstruction.

4.3 Detecting Caustics

Because passing through a caustic implies overturning of the zero level set in the x-θ space, the number of θ's satisfying $\phi(z, x, \theta(x, z)) = 0$ will increase or decrease by two when x varies monotonically. Therefore, a simple way to detect caustics is first enumerating the number of roots θ_k's for every x_i, then checking where those numbers have sudden jumps, and finally approximating locations of caustics by taking the mid-point of two adjacent x_i's which have different numbers of θ_k. The resulting approximation of the caustics locations is of first-order accuracy.

Let x_c^* be the exact location of a caustic at some fixed z^*. Assume that x_c is the computed caustic location obtained from the level set formulation, i.e. solving

$$\phi(z^*, x, \theta(x, z^*)) \quad = \quad 0, \tag{51}$$

$$\phi_\theta(z^*, x, \theta(x, z^*)) \quad = \quad 0. \tag{52}$$

Let x_c' be the approximate caustic location computed using our mid-point approximation. We have at least $x_c = x_c^* + O(\Delta x^2)$ which is delivered by the second order scheme used here. Because the distance between x_c and x_c' is less than $\Delta x/2$, we have $x_c' = x_c + O(\Delta x)$ and, therefore, $x_c' = x^* + O(\Delta x)$.

In terms of multivalued traveltimes, passing through a caustic implies that the number of traveltimes increases or decreases by two as we will see in numerical examples.

4.4 Local Level Set Method for Traveltime and Amplitude

The computational complexity of the above algorithm can be improved dramatically by implementing a narrow banding [1] or PDE based version [28] of the local level set method. In this work we adopt a version similar to the one proposed in [28].

The updates in Algorithm 1 require computations for all grid points in the domain. But this is not necessary because the only information we will extract from the data is the zero level set defined by $\phi = 0$. This means the cost of the above algorithm can be reduced by updating the level set function, ϕ, the traveltime function, T, and the quantities ϕ_x, ϕ_θ and Δ locally around only the zero level set of ϕ. Because we are only interested in the zero level set, all the updates can actually be done in a tube centered at $\phi = 0$. The radius of this tube, γ, is picked to be $5\Delta x$, due to the fact that 5 grid values are needed for the fifth order WENO scheme when solving the advection equations. Therefore, by only considering the grid points within this tube, the complexity of the above algorithm can be reduced by a factor of N to $O(N^2 LogN)$.

Next we have to initialize the quantities that we are going to advect. At $z = 0$, we can set ϕ_x and ϕ_θ equal to 1 and 0 respectively. However, ψ_x is singular at the source and it is better to start computing ψ_x and ψ_θ at some $z = dz > 0$ close to zero. Assuming that the velocity c can be approximated by a constant near the source, we have

$$\begin{aligned} \psi_x(z,x,\theta)|_{z=dz} &= \frac{\cos^2\theta}{dz}, \\ \psi_\theta(z,x,\theta)|_{z=dz} &= 1. \end{aligned} \tag{53}$$

Thus at small $z = dz > 0$,

$$\phi(z,x,\theta)|_{z=dz} = x - \tan(\theta)\cdot dz, \tag{54}$$

and $\Delta(dz,x,\theta) \equiv -2$, which is independent of the dz as long as the velocity can be well approximated by a constant near the source. This makes the computation of amplitude stable.

Hence we have a new algorithm for computing the geometrical optics term.

Algorithm 2:

I. Initialization.

1. Given N_x and N_θ, determine

$$\Delta x = \frac{x_{\max} - x_{\min}}{N_z - 1} \text{ and } \Delta\theta = \frac{2\theta_{\max}}{N_\theta - 1}.$$

2. Initialize ϕ, T, ϕ_x and ϕ_θ at $z = 0$.
3. For each (x_i, θ_j), where $i = 1, \ldots, N_x$ and $j = 1, \ldots, N_\theta$, check if any of $|\phi(x_i,\theta_j)|$, $|\phi(x_{i-1},\theta_j)|$, $|\phi(x_{i+1},\theta_j)|$, $|\phi(x_i,\theta_{j-1})|$ or $|\phi(x_i,\theta_{j+1})|$ is less than γ. Collect all these points into the set Γ.

II. March in z until $z = z_{\max}$.

1. Determine Δz from the CFL condition.
2. March one Δz step by solving the level set equation (25) in Γ.
3. Reinitialize the level set function in Γ by solving (45).
4. March one Δz step by solving the traveltime equation (31) in Γ.
5. If $z \neq \Delta z$, update Δ by solving equation (41).
6. Orthogonalize T, ϕ_x and ϕ_θ to ϕ, respectively, in Γ by solving equation (48).
7. If $z \neq \Delta z$, orthogonalize Δ to ϕ in Γ. Otherwise, initialize Δ.
8. Update the tube Γ.
9. Detect caustics by checking if there is a change in the number of θ_k's which gives $\phi(z; x_i, \theta_k) = 0$ for two adjacent points x_i.

III. Output. For each x_i with $i = 1, \ldots, N_x$,

1. Determine **all** roots θ_k such that $\phi(z_{\max}; x_i, \theta_k) = 0$ $(k = 1, \cdots)$.
2. Determine $T(z_{\max}; x_i, \theta_k)$ $(k = 1, \cdots)$ by interpolation.
3. Determine $\phi_x(z_{\max}, x_i, \theta_k)$, $\phi_\theta(z_{\max}; x_i, \theta_k)$ and $\Delta(z_{\max}; x_i, \theta_k)$ $(k = 1, \cdots)$ by interpolation, and then compute $A(z_{\max}; x_i, \theta_k)$.

To determine Δz in step II.1, we only need to scan through the grid points in the computational tube Γ in order to determine the maxima of velocity fields u and v, and this takes $O(NLogN)$ steps.

Unlike the global level set method, the reinitialization step in II.3 is used not only to make the level set function more regular but also to ensure the location of the tube in Step II.8 more accurate. This step is necessary here and the number of iterations is to be determined so that the information of the location of the zero level set is propagated by a distance larger than γ, the radius of the tube. Numerically, one or two steps per iteration in z would be enough to get a reasonably good solution. However, formally, let β be the CFL number used in the reinitialization and $m_{\min}$ be the minimum number of iterations of reinitialization; then we have

$$m_{\min} = \frac{\gamma}{\beta \min(\Delta x, \Delta\theta)}. \tag{55}$$

Because $\gamma = O(\Delta x)$, $m_{\min} = O(1)$. The overall complexity of the reinitialization step for each Δz advancement is equal to the number of grid points within the tube and is given by $O(NLogN)$.

On the other hand, there is no need to extend the traveltime, the derivatives of ϕ and the quantity Δ from the zero level set throughout the whole tube because the purpose of the orthogonalization is to reduce the error generated in the interpolation step III.2 and III.3 as mentioned before. Therefore, one or two iterations per marching step are sufficient.

Next issue is how to update the computational tube Γ. A simple way is to scan all grid points in the domain and to apply the same procedure as that in I.3. The complexity of the

Δx	l_1 error	l_1 order	l_2 error	l_2 order	l_∞ error	l_∞ order
0.20000	0.01044350		0.01077493		0.01504211	
0.10000	0.00580110	0.8482	0.00540664	0.9948	0.00678677	1.1482
0.05000	0.00193626	1.5830	0.00251217	1.5640	0.00251217	1.4337
0.02500	0.00050419	1.9412	0.00047756	1.9369	0.00069198	1.8601
0.01250	0.00011634	2.1156	0.00011220	2.0895	0.00017029	2.0227
0.00625	0.00002791	2.0592	0.00002721	2.0435	0.00004292	1.9882

Table 1: Accuracy and convergence order of traveltimes in Example 1 at $z = 1$ km.

resulting method will be $O(N^2)$. However, because the motion of the zero level set is purely advective, zeros will not be generated outside the tube. We can, therefore, update the tube by only scanning through the boundary of Γ, and this requires only $O(NlogN)$ operations.

As a result, each substep in II can be done within $O(NLogN)$ calculations. Therefore, for each iteration in z-direction, the complexity is $O(NLogN)$. Because of the CFL condition, the number of iterations in z is of $O(N)$. Overall the complexity of this algorithm is only $O(N^2LogN)$. Comparing to $O(N^4)$ as typically seen in the Lagrangian ray tracing method, this Eulerian method is highly efficient and attractive.

5 Numerical Examples

For the first three examples, we put a point source at the origin and velocity functions $c(x, z)$ are all C^∞. The fourth example, the synthetic Marmousi model, is a challenging one where the velocity function is given only as gridded values. Unless specified, the computational domain we use in the following examples is chosen to be

$$\Omega_p = \{(x, \theta) : -1 \le x \le 1, \theta_{\max} \le \theta \le \theta_{\max}\} \ . \tag{56}$$

where $\theta_{\max} = 9\pi/20$. The Marmousi velocity will be rescaled to the above computational domain accordingly.

5.1 Constant model

The simplest case one can imagine is the constant velocity model with $c(x, z) = 1$. Figure 1 shows the exact and computed traveltimes and amplitudes of the constant model. The solid lines are the exact solutions. The numerical solutions match well with the true values.

Tables 1 and 2 show the convergence results for this test case. Convergence history for traveltimes is shown in Table 1, while Table 2 contains that of the amplitudes. The results show second-order convergence for both traveltimes and amplitudes at z=1.

In this simple case, we can also compute the solution by assuming that the boundary $x = x_{\max}$ is reflective. When the zero level set hits the boundary $x = x_{\max}$ in the x-θ space,

Δx	l_1 error	l_1 order	l_2 error	l_2 order	l_∞ error	l_∞ order
0.20000	0.00093010		0.00091941		0.00123784	
0.10000	0.00052955	0.8126	0.00049836	0.8835	0.00061722	1.0039
0.05000	0.00016404	1.6907	0.00015484	1.6863	0.00020976	1.5570
0.02500	0.00004076	2.0086	0.00003870	2.0000	0.00005544	1.9195
0.01250	0.00000970	2.0709	0.00000930	2.0568	0.00001391	1.9944
0.00625	0.00000261	1.8924	0.00000253	1.8735	0.00000382	1.8623

Table 2: Accuracy and convergence order of amplitudes in Example 1 at $z = 1$ km.

it will not leave the domain; instead, a new ray will be generated in the computational space at the same location $x = x_{\max}$ and with θ having opposite sign to the original ray.

For the traveltime, we have to determine boundary conditions for the incident and the reflected rays separately. We can use the same boundary condition as in the non-reflective case for the incident ray. The reflective ray has the same traveltime as the incident ray at the boundary $x = x_{\max}$.

Therefore, we have the following boundary condition on $x = x_{\max}$,

$$\begin{aligned}
\phi(x_{\max}, \theta) &= \phi(x_{\max}, -\theta) \\
\phi_x(x_{\max}, \theta) &= \phi_x(x_{\max}, -\theta) \\
\phi_\theta(x_{\max}, \theta) &= \phi_\theta(x_{\max}, -\theta) \\
\Delta(x_{\max}, \theta) &= \Delta(x_{\max}, -\theta) \\
T(x_{\max}, \theta) &= \begin{cases} \text{from (43)} & \text{if } u(x_{\max}, \theta) > 0 \\ T(x_{\max}, -\theta) & \text{if } u(x_{\max}, \theta) < 0 \end{cases}
\end{aligned} \tag{57}$$

Similar boundary conditions can be used on the other side $x = x_{\min}$ and will not be fully discussed here. For the other two boundaries $\theta = \theta_{\max}$ and $\theta = -\theta_{\max}$, we can use the same boundary conditions as in the non-reflective case detailed in the previous section.

Figures 2 and 3 show solutions obtained at z=1 using the proposed method with reflective boundary conditions imposed on both boundaries $x = \pm 1$. Figure 2 shows seven segments of zero level set curves; they correspond to seven branches of traveltimes and amplitudes in the physical domain. Multiple reflections are captured clearly as shown in Figure 3 for traveltimes and amplitudes using 120 grid points in both x and θ directions.

5.2 Wave guide model

The velocity function is given by

$$c(x, z) = 1.1 - \exp(-0.5x^2)\,. \tag{58}$$

The function is symmetric with respect to $x = 0$, and we also expect the same type of symmetry in both the traveltime and the amplitude.

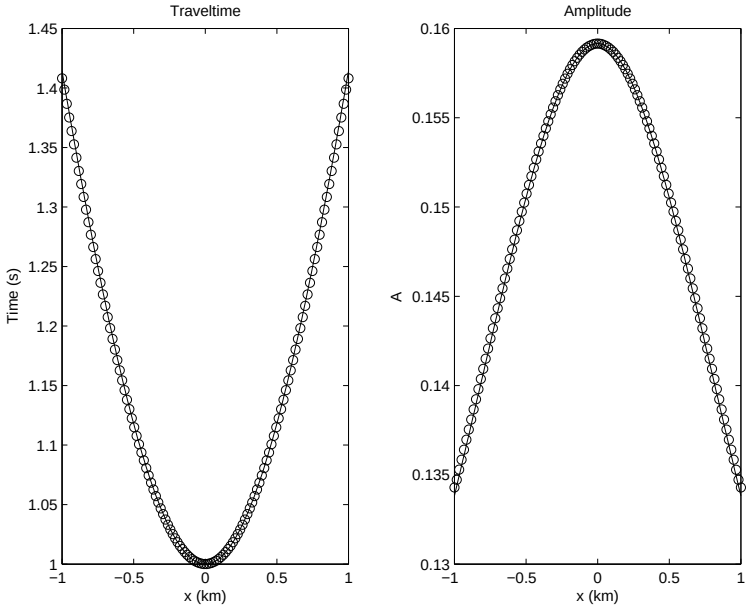

Figure 1: Traveltimes and amplitude at $z = 1$ (km) in the constant model using a 120-by-120 grid. Solid line: the exact solution. Circles: the solution using the local level set method.

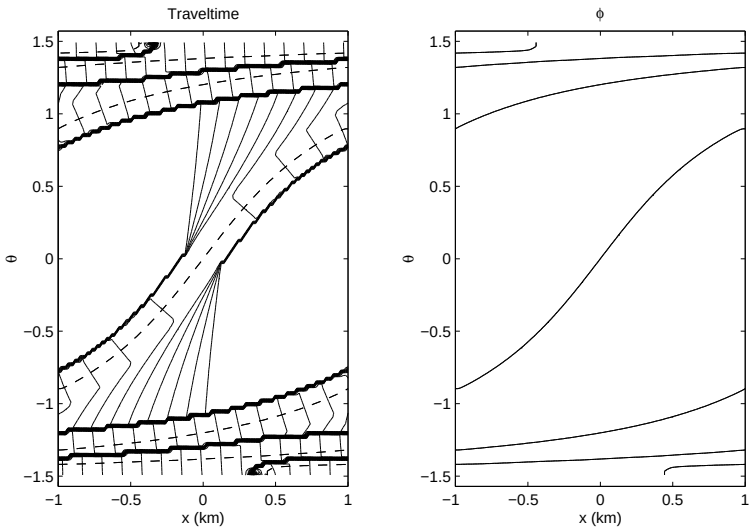

Figure 2: Contours of the traveltime and the zero level set at $z = 0.75$km in the constant model using a 120-by-120 grid with reflective boundary conditions.

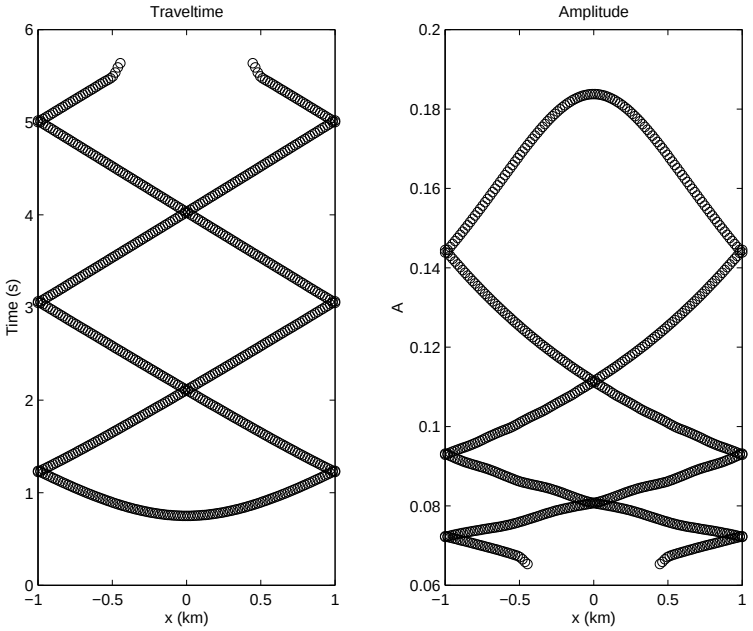

Figure 3: Traveltime at $z = 0.75$km with reflective boundary conditions in the constant model.

Figure 4 shows the zero level set overlaying the traveltime field at $z = 1.6$ using a 120×120 grid in the x-θ space. The dashed line is the location of the zero level set and the solid lines are contours of the traveltime field T. There are discontinuities in the traveltime field coming from the update within the computational tube. However, since we only use the information near the dashed line, the jumps in T will not interfere with the interpolation as long as these jumps are at least one grid distance away from the zero level set. Theoretically, to resolve the zero level set itself on a given mesh, two parallel level set segments should be greater than one Δx distance away from each other so that they can be resolved. In our computation here, we need to perform the orthogonalization procedure, and the normals from the two parallel level set segments intersect in the middle so that discontinuities appear in the traveltime field. To avoid discontinuities interfering with our computation, we have to keep discontinuities away from the zero level set at least one Δx away. This in turn requires that the computational mesh resolve the parallel segments of the zero level set greater than $2\Delta x$ distance away. At the tip of the zero level set, the traveltime is continuous along the zero level set, so discontinuities in the traveltime field will not hurt the computation. Computationally, due to the smearing of discontinuities, the required mesh may be finer.

Notice also that the contours are perpendicular to the zero level set as designed. As z varies, the zero level set is advected so that it has more turnarounds and the number of traveltime arrivals increases from 1 to 3.

The solutions in Figures 5 and 6 show traveltimes, amplitudes and some intermediate quantities at z =1.6 using 120-by-120 and 240-by-240 grid points, respectively. The solid lines in the traveltime and amplitude plots are obtained using a ray tracing method. The

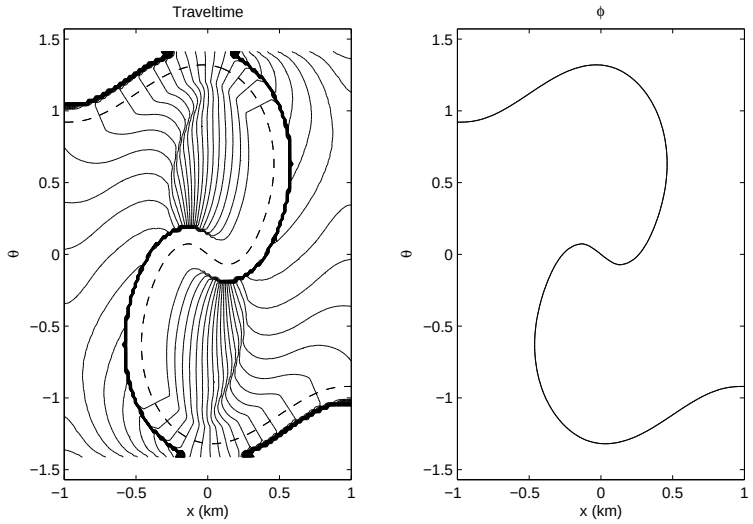

Figure 4: Contours of the traveltime and the zero level set in the waveguide model using a 120-by-120 grid at $z = 1.6$km.

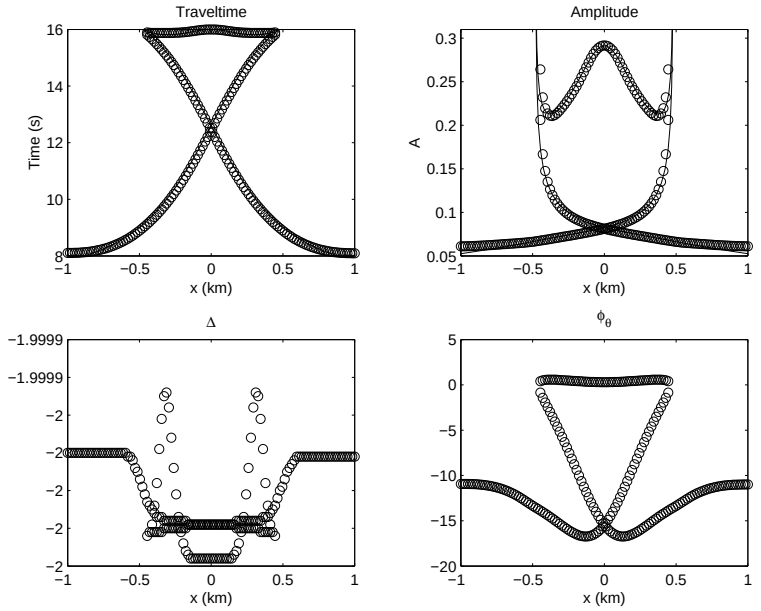

Figure 5: Traveltime, amplitude, Δ and ϕ_θ at $z = 1.6$km in the waveguide model using a 120-by-120 grid.

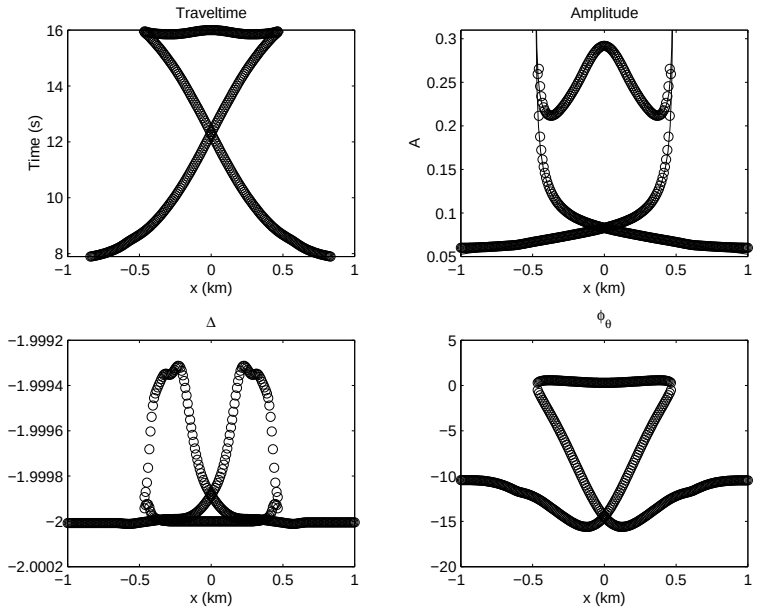

Figure 6: Traveltime, amplitude, Δ and ϕ_θ at $z = 1.6$km in the waveguide model using a 240-by-240 grid.

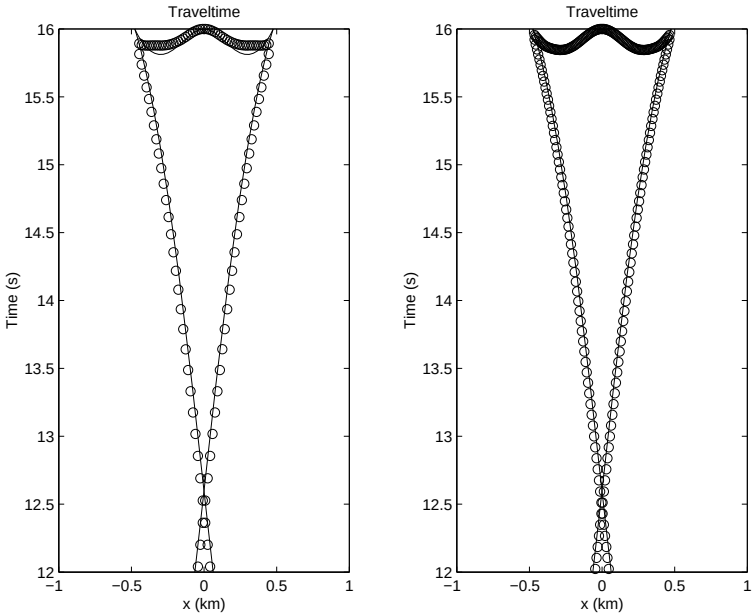

Figure 7: Traveltime at $z = 1.6$km in the waveguide model using 120-by-120 and 240-by-240 grids (circles) vs. traveltime by a ray tracing method (solid line).

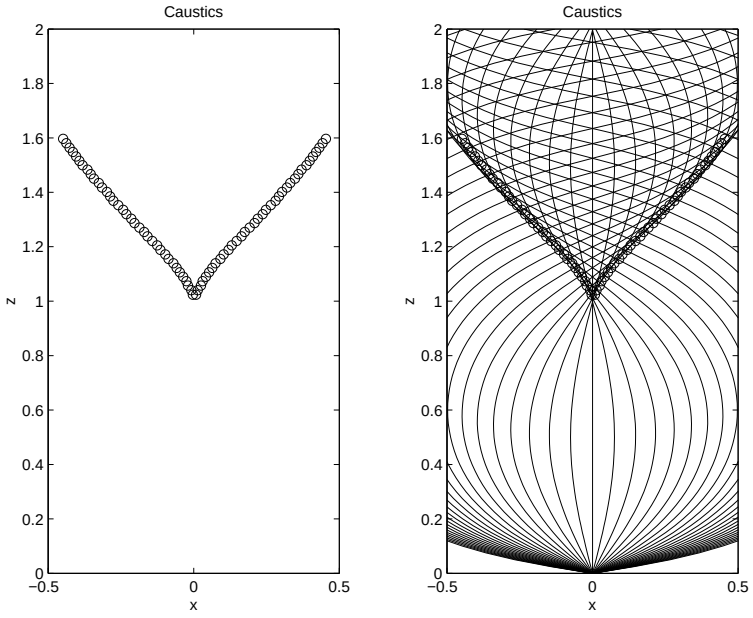

Figure 8: Location of caustics and some rays from a ray tracing method in the waveguide model. Caustics are determined by the local level set method with a 360-by-360 grid in the x-θ space.

solutions are symmetric as expected. Comparisons between the solution from the Eulerian method and that from a ray tracing method are also shown in Figure 7. As we mentioned earlier, the velocity model is approximated by a constant near the source and this gives the initial condition $\Delta = -2$ at z=dz. For this waveguide model, because u_x=v_θ=0, the equation for Δ is purely advective; therefore the exact solution is $\Delta(z; x, \theta)$=-2, which is independent of z. The variations in the subplots of Δ in Figures 5 and 6 are due to numerical errors.

The singularities in the amplitudes, shown in upper right subfigures in Figures 5 and 6, come from the vanishing of ϕ_θ on the zero level set of ϕ, shown in lower right subfigures in Figures 5 and 6 respectively, at around $x = \pm 0.45$.

The caustic curves detected by the local level set method are shown in Figure 8: circles are computed locations of the caustics in the waveguide model, and the solid lines are the rays emanating from the source computed by a ray tracing method. The caustic locations are exactly those places where rays form an envelop as seen in the figure.

5.3 Sinusoidal model

This example is adapted from the sinusoidal waveguide model used in [35, 36], and the velocity function is given by

$$c(x, z) = 1 + 0.2 \sin(0.5\pi z) \sin[3\pi(x + 0.55)] \,. \tag{59}$$

The zero level set and the contours of the traveltime field by a 120 by 120 grid in x-θ space

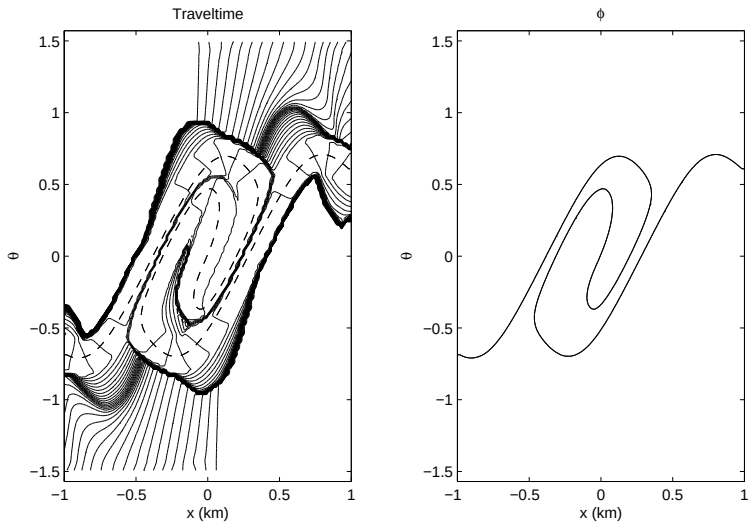

Figure 9: Contours of the traveltime and the zero level set at $z = 2.0$km in the Sinusoidal model by a 120-by-120 grid.

at $z = 2.0$ are given in Figure 9. As remarked above, the traveltime function is only updated within a tube around the zero level set, and the discontinuity in the traveltime field is clearly seen in the left subfigure of Figure 9. Figures 10 and 11 show traveltimes, amplitudes and some intermediate quantities at z =2.0 using 120-by-120 and 240-by-240 grids, respectively. The subplots for traveltimes in Figures 10 and 11 show that the triplications in the traveltime developed at z=2.0 are clearly captured by the level set Eulerian method. Singularities in the amplitude come from the overturning of the zero level set in the phase space, i.e. $\phi_\theta = 0$, which is shown in the lower right subfigure in Figures 10 and 11. Close-up in the triplication region is shown in Figure 12: solutions from the level set method are shown in circles while solutions from the ray tracing method are shown in dots.

Figure 13 shows locations of the caustics detected by the proposed method, and the results match with that from the ray tracing method.

5.4 Synthetic Marmousi model

This example is the Marmousi model from the 1996 INRIA Workshop on Multi-arrival Traveltimes. The calibration data used here were computed by Dr. Klimes and can be found at http://www.caam.rice.edu/∼benamou/traveltimes.html. This is a synthetic model which will challenge the level set method used here.

The original Marmousi model is sampled on a 24m by 24m grid, consisting of 384 samples in the x-direction and 122 samples in the z-direction; therefore the model dimension is 9.192km long in the x-direction and 2.904km deep in the z-direction. In the computational results presented here, we use a portion of Marmousi model, i.e., a window from 2.64km to 9.36km in the x-direction and from 0km to 2.904km in the z-direction. The source is located

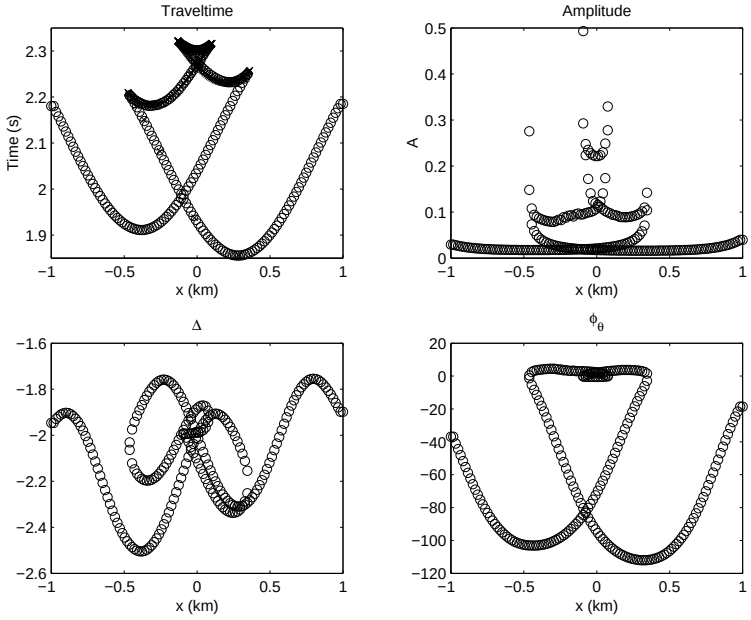

Figure 10: Traveltime, amplitude, Δ and ϕ_θ at $z = 2.0$km in the Sinusoidal model using a 120-by-120 grid.

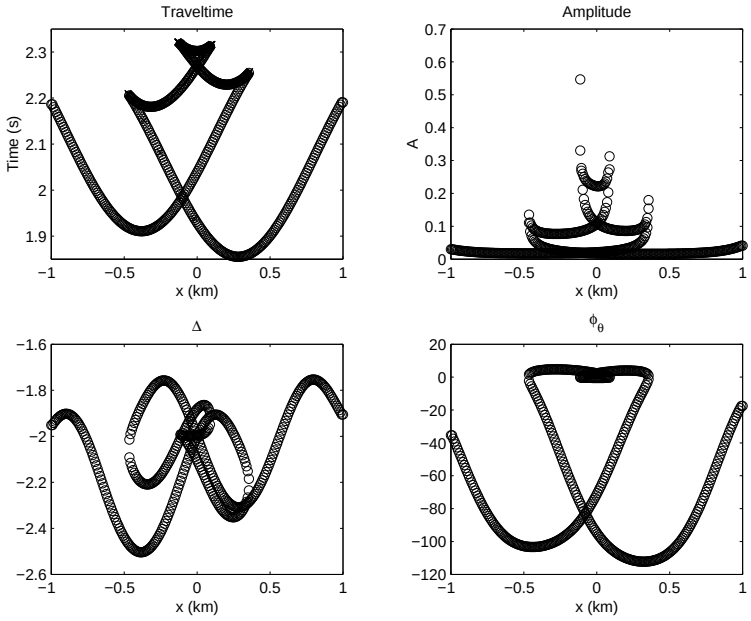

Figure 11: Traveltime, amplitude, Δ and ϕ_θ at $z = 2.0$km in the Sinusoidal model using a 240-by-240 grid.

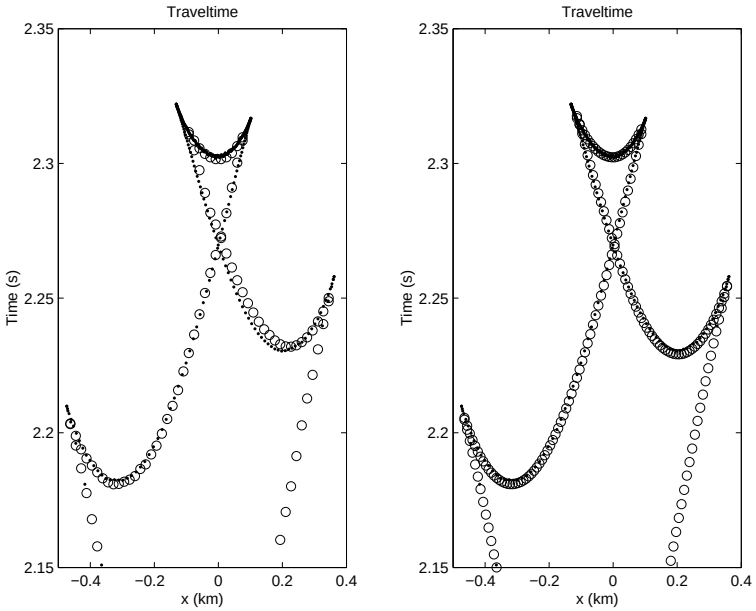

Figure 12: Traveltime at $z = 2.0$ km in the Sinusoidal model using 120-by-120 and 240-by-240 grids (circles) vs. traveltime by a ray tracing method (dots).

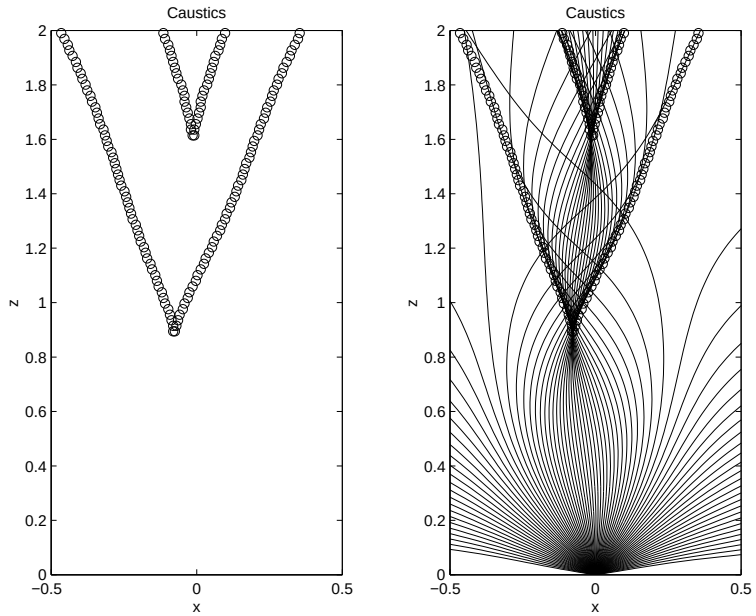

Figure 13: Location of caustics and some rays from a ray tracing method in the Sinusoidal model. Caustics are determined by the local level set method with a 360-by-360 grid in the x-θ space.

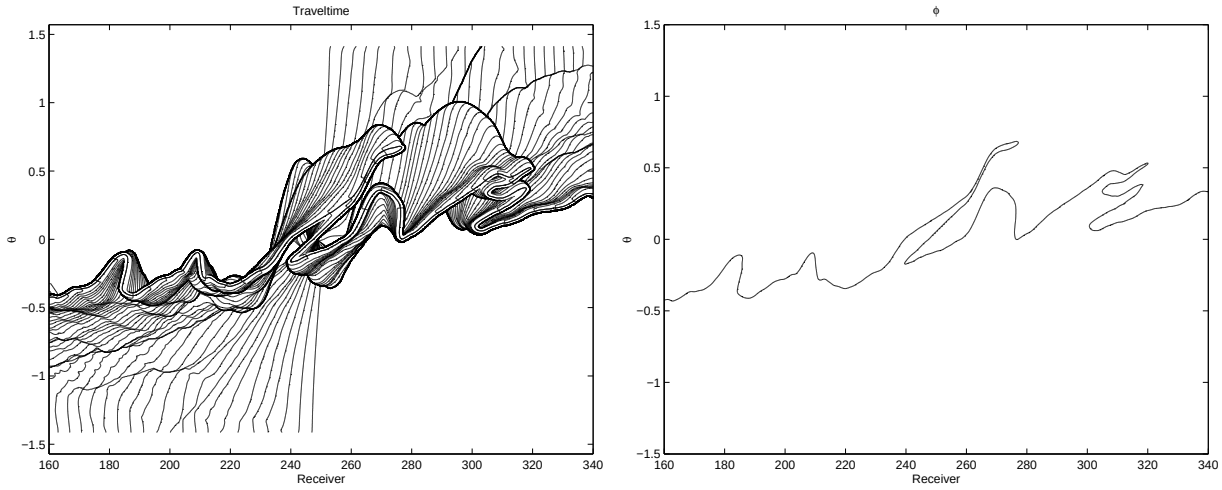

Figure 14: Contours of the traveltime and the zero level set in the Marmousi model at $z = 0.0$km.

at x=6.0km and z=2.8km. The purpose is to compute (possibly multivalued) traveltimes for those sampling points, i.e. the receivers from 160 to 340 on the surface z=0.0km. Since we are using a local level set method, we can choose such a large window of the velocity model. In the example presented in [30], we were able to deal with a much smaller portion of the velocity model because there we used a global level set method.

As illustrated in [30], to resolve a complicated wavefront like the one generated by the Marmousi model, we have to use very fine computational meshes which need huge memory storage in the global level set setup. With the local level set method developed here, we are able to tackle a larger portion of the original velocity with reasonable memory and computational cost. Figure 14 shows the zero level set and its overlay on the traveltime field; in this computation we have refined the orginal model with a refinement ratio =8, and set reinitializaton and orthogonalization steps being 15, respectively. As we can see from the plot, the zero level set has lots of overturnings and tiny tips. Therefore, there are lots of caustics developed in the wave propagation. The resulting traveltimes at the surface along with the ray tracing solutions are shown in Figure 15; the two solutions match with each other nicely. Figures 16-18 show zoom-in details at some particular locations. Near Receiver 310, we have captured five branches of traveltimes; this can be seen from both the zero level set in Figure 14 and the traveltime branches in Figure 16. Near Receivers 272 and 182, we have captured three branches of traveltimes; in particular, the branches in Figure 17 are tiny which illustrate the high resolution of the proposed level set method.

6 Conclusion

We have proposed a local level set method for paraxial geometrical optics, so that the multivalued traveltime and amplitude can be constructed with ease. The computational complex-

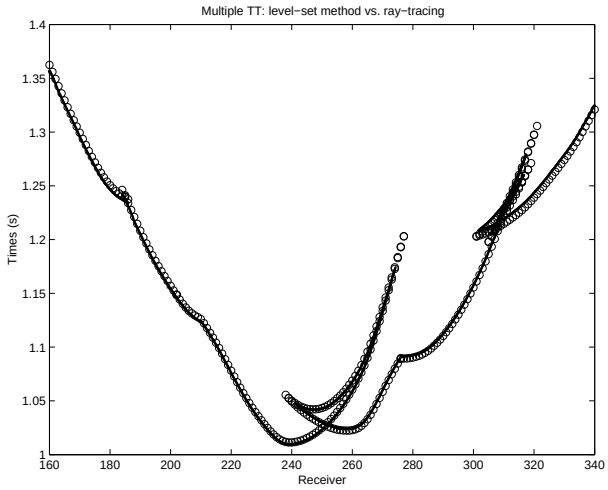

Figure 15: Comparison between traveltimes using a ray tracing method and the local level set method at $z = 0.0$km in the Marmousi model.

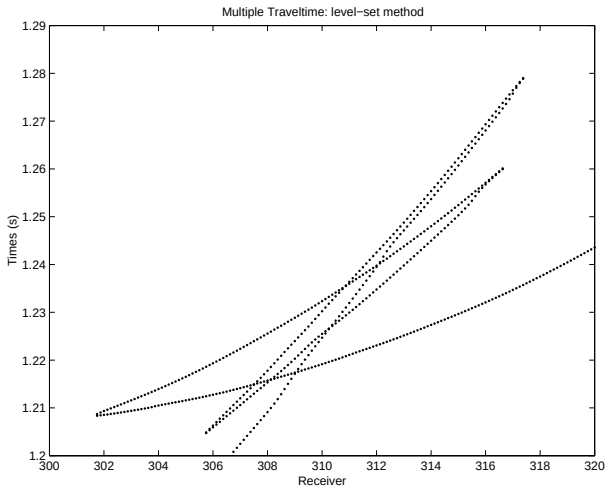

Figure 16: Zoom-in at Receiver 310: five branches of traveltimes by the local level set method at $z = 0.0$km in the Marmousi model.

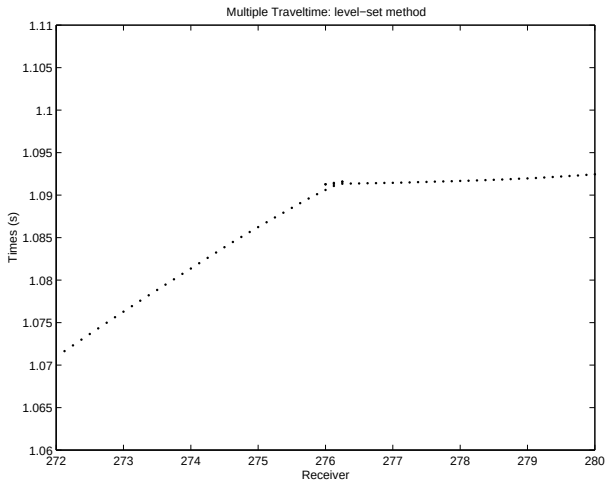

Figure 17: Zoom-in at Receiver 272: tiny three branches of traveltimes by the local level set method at $z = 0.0$km in the Marmousi model

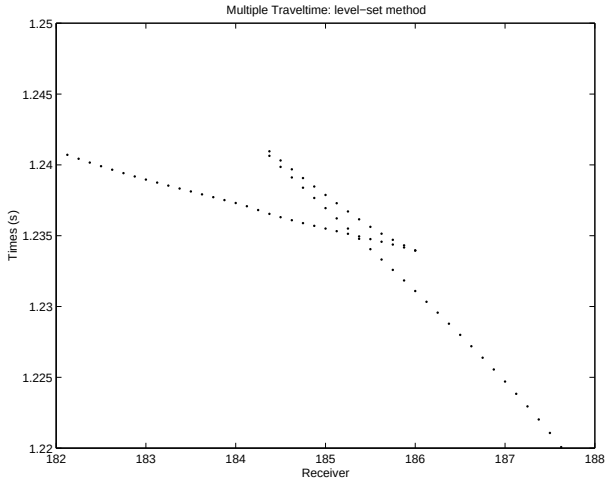

Figure 18: Zoom-in at Receiver 182: three branches of traveltimes by the local level set method at $z = 0.0$km in the Marmousi model.

ity of the algorithm is $O(N^2 logN)$, therefore it is highly efficient. Although the subhorizontal condition is required for the approach to work, it is suitable for many applications, such as reflection seismics, underwater acoustics and optics. The future work includes grafting this approach to high resolution seismic inversion [34] and computing the high frequency wave field using a time domaim approach proposed in [6] rather than the usual frequency domain approach in [23].

Acknowledgment

J. Qian thanks Professors R. Burridge, B. Cockburn, S. Osher, F. Reitich and W. W. Symes for helpful discussions. J. Qian and S. Leung were supported by ONR Grant #N00014-02-1-0720.

References

[1] D. Adalsteinsson and J.A. Sethian. A fast level set method for propagating interfaces. *J. Comput. Phys.*, 118:269–277, 1995.

[2] J.-D. Benamou. Direct solution of multi-valued phase-space solutions for Hamilton-Jacobi equations. *Comm. Pure Appl. Math.*, 52:1443–1475, 1999.

[3] J. D. Benamou. An introduction to Eulerian geometrical optics (1992 - 2002). *J. Sci. Comp.*, 19:63–93, 2003.

[4] J.-D. Benamou and I. Solliec. A Eulerian method for capturing caustics. *J. Comput. Phys.*, 162:132–163, 2000.

[5] M. Born and E. Wolf. *Principles of optics.* The Macmillan Company, 1964.

[6] R. Burridge. Asymptotic evaluation of integrals related to time-dependent fields near caustics. *SIAM J. Appl. Math.*, 55:390–409, 1995.

[7] R. Burridge, M. V. de Hoop, D. Miller, and C. Spencer. Multiparameter inversion in anisotropic media. *Geophys. J. Internat.*, 134:757–777, 1998.

[8] L.-T. Cheng, H. Liu, and S. J. Osher. High frequency wave propagation in Schrodinger equations using the level set method. Preprint (www.levelset.com), 2003.

[9] L.-T. Cheng, S. J. Osher, and J. Qian. Level set based eulerian methods for multivalued traveltimes in both isotropic and anisotropic media. In *73st Ann. Internat. Mtg., Soc. Expl. Geophys., Expanded Abstracts*, pages 1801–1804. Soc. Expl. Geophys., Tulsa, OK, 2003.

[10] B. Engquist and O. Runborg. Computational high frequency wave propagation. In *Acta Numerica, Pages 1-86.* Cambridge University Press, Cambridge, United Kingdom, 2003.

[11] B. Engquist, O. Runborg, and A-K Tornberg. High frequency wave propagation by the segment projection method. *J. Comp. Phys.*, 178:373–390, 2002.

[12] L. C. Evans. Towards a quantum analogue of weak KAM theory. Preprint, 2002.

[13] S. Fomel and J. Sethian. Fast phase space computation of multiple traveltimes. *Proc. Nat. Aca. Sci.*, 99:7329–7334, 2002.

[14] S. Geoltrain and J. Brac. Can we image complex structures with first-arrival traveltime. *Geophysics*, 58:564–575, 1993.

[15] L. Gosse. Using K-branch entropy solutions for multivalued geometric optics computations. *J. Comput. Phys.*, 180:155–182, 2002.

[16] S. Gray and W. May. Kirchhoff migration using eikonal equation traveltimes. *Geophysics*, 59:810–817, 1994.

[17] G. S. Jiang and D. Peng. Weighted ENO schemes for Hamilton-Jacobi equations. *SIAM J. Sci. Comput.*, 21:2126–2143, 2000.

[18] S. Jin and X. Li. Multi-phase computations of the semi-classical limit of the Schrodinger equation and related problems. Physica D (in press), 2003.

[19] S. Jin and S. Osher. A level set method for the computation of multivalued solutions to quasi-linear hyperbolic PDEs and Hamilton-Jacobi equations. Preprint (www.levelset.com), 2003.

[20] J. B. Keller. Semiclassical mechanics. *SIAM Review*, 27:485–504, 1985.

[21] J. B. Keller and R. M. Lewis. Asymptotic methods for partial differential equations: the reduced wave equation and Maxwell's equations. *Surveys in Applied Mathematics*, 1:1–82, 1995.

[22] P. L. Lions. *Generalized solutions of Hamilton-Jacobi equations.* Pitman Advanced Publishing Program, 1982.

[23] D. Ludwig. Uniform asymptotic expansions at a caustic. *Comm. Pure Appl. Math.*, XIX:215–250, 1966.

[24] S. Operto, S. Xu, and G. Lambare. Can we image quantitatively complex models with rays. *Geophysics*, 65:1223–1238, 2000.

[25] S. Osher, L.-T. Cheng, M. Kang, H. Shim, and Y-H Tsai. Geometrical optics in a phase space based level set and Eulerian framework. *J. Comput. Phys.*, 179:622–648, 2002.

[26] S. Osher and R. P. Fedkiw. *The Level Set Method and Dynamic Implicit Surfaces.* Springer-Verlag, New York, 2002.

[27] S. J. Osher and C. W. Shu. High-order Essentially NonOscillatory schemes for Hamilton-Jacobi equations. *SIAM J. Num. Anal.*, 28:907–922, 1991.

[28] D. Peng, B. Merriman, S. Osher, H. K. Zhao, and M. Kang. A pde-based fast local level set method. *J. Comput. Phys.*, 155:410–438, 1999.

[29] J. Qian, L.-T. Cheng, and S.J. Osher. A level set based Eulerian approach for anisotropic wave propagations. *Wave Motion*, 37:365–379, 2003.

[30] J. Qian and S. Leung. A level method for paraxial multivalued traveltimes. Submitted to J. Comp. Phys.; UCLA CAM report 03-28, 2003.

[31] J. Qian and W. W. Symes. Adaptive finite difference method for traveltime and amplitude. *Geophysics*, 67:167–176, 2002.

[32] S. J. Ruuth, B. Merriman, and S. J. Osher. A fixed grid method for capturing the motion of self-intersecting interfaces and related PDEs. *J. Comput. Phys.*, 151:836–861, 1999.

[33] J. Steinhoff, M. Fan, and L. Wang. A new Eulerian method for the computation of propagating short acoustic and electromagnetic pulses. *J. Comput. Phys.*, 157:683–706, 2000.

[34] W. W. Symes. Mathematics of reflection seismology. In *Annual Report, The Rice Inversion Project, (http://www.trip.caam.rice.edu/).* Rice University, 1995.

[35] W. W. Symes. A slowness matching finite difference method for traveltimes beyond transmission caustics. In *68th Ann. Internat. Mtg., Soc. Expl. Geophys., Expanded Abstracts*, pages 1945–1948. Soc. Expl. Geophys., 1998.

[36] W. W. Symes and J. Qian. A slowness matching Eulerian method for multivalued solutions of eikonal equations. *J. Sci. Comp.*, 19:501–526, 2003.

[37] W. W. Symes, R. Versteeg, A. Sei, and Q. H. Tran. Kirchhoff simulation, migration and inversion using finite difference traveltimes and amplitudes. In *Annual Report, The Rice Inversion Project, (http://www.trip.caam.rice.edu/).* Rice University, 1994.

[38] R. Thom. *Structural stability and morphogenesis.* Benjamin, New York, 1975.

[39] J. van Trier and W. W. Symes. Upwind finite-difference calculation of traveltimes. *Geophysics*, 56:812–821, 1991.

[40] J. Vidale. Finite-difference calculation of travel times. *Bull., Seis. Soc. Am.*, 78:2062–2076, 1988.

[41] V. Vinje, E. Iversen, and H. Gjystdal. Traveltime and amplitude estimation using wavefront construction. *Geophysics*, 58:1157–1166, 1993.

[42] B. S. White. The stochastic caustic. *SIAM J. Appl. Math.*, 44:127–149, 1984.

[43] B. S. White. Wave action on currents with vorticity. *J. Fluid Mech.*, 386:329–344, 1999.

[44] L. Zhang. *Imaging by the wavefront propagation method.* PhD thesis, Stanford University, Stanford, CA94305, 1993.

[45] H.-K. Zhao, T. Chan, B. Merriman, and S. J. Osher. A variational level set approach for multiphase motion. *J. Comput. Phys.*, 127:179–195, 1996.